数理解析研究所講究録
974巻 1996年 164-169

Two-Dimensional Study of Flow past a Circular Cylinder

Masanori Hashiguchi
Institute of Computational Fluid Dynamics
1-22-3 Haramachi, Meguro-ku, Tokyo 152, Japan

Kunio Kuwahara
The Institute of Space and Astronautical Science
3-1-1 Yoshinodai, Sagami-hara, Kanagawa 229, Japan

Abstract

Two-dimensional computations of flow around a circular cylinder were carried out by integrating the incompressible Navier-Stokes equations. The multi-directional third-order upwind finite-difference method was utilized to discretize the fundamental equations. No explicit turbulence model was used. Flow computations were performed for a wide range of Reynolds numbers(Re = 0.1 - 10^6). Results are compared to those from other theoretical and experimental works. It is found that the present method can predict the dependence of the flow field on the Reynolds number(i.e., by its accurate prediction of the drag crisis, the separation points , the streamlines and the pressure distribution). Based on the results, it can be concluded that around the drag crisis, the flow past a circular cylinder approaches a potential flow and the related vortex shedding pattern from the cylinder surface takes a quite different pattern.

1. Introduction

From the fluid mechanics, hydraulics and wind engineering points of view, the flow past a circular cylinder has been the subject of numerous experimental and numerical studies because:(i) this type of flow exhibits fundamental mechanisms, and (ii) its numerous industrial applications; for example, when designing the shape of a aerodynamic body, it is of great importance to understand how the dynamic force is generated. To achieve the goal of obtaining a detailed information of the flow field being investigated, computational fluid dynamics(CFD) has emerged as an attractive, powerful tool in many designing process.

Chronologically, the first study concerning the steady flow past a circular cylinder was reported by Thom[1], in 1933, for Reynolds number of 10 and 20. In the late 50's, the works of Kawaguti[2] and Payne[3] were restricted to low Reynolds number(Re = 40) and relatively low Reynolds numbers(Re = $40-100$), respectively. In the following 30 years, a great number of computational studies, devoted to this type of flow, made their apperance in the literature but the results were limited to a very narrow range of Reynolds number($Re = 40-10^3$). In 1984, Kawamura and Kuwahara[4] presented computations at high Reynolds number($Re = 10^3-10^5$) for flow around a circular cylinder with surface roughness. By introducing a new third-order upwind scheme, they solved the incompressible Navier-Stokes equations without incorporating a turbulence model. Their computations where the first to reproduce the drag crisis phenomenon but, due to the introduction of the surface roughness, the value of the critical Reynolds number was lower when compared with that of the smooth circular cylinder. Tamura and Kuwahara[5] performed the two-dimensional computation for the smooth surface circular cylinder. However, they could not reproduce the sharp decrease in the drag curve as it is observed experimentally. In the same paper, when their computations were extended to three dimensions, the results showed a very good agreement with the experimental data in both the subcritical and supercritical regime. Even the importance of three-dimensional effect was recognized, there was still the question whether the two-dimensional flow assumption will hold or not when a more accurate discretization method is employed. In 1985, Ishii et al.[6] had simulated a two-dimensional flow based on an high accurate scheme for compressible flow, showing quantitatively good agreement in the prediction of the drag coefficient around the critical regime at a Mach number equals to 0.3. Unfortunately, this scheme is insufficient for the computation of low speed flows because of the well-known compressible limit. Recently, in order to improve the accuracy in the computation of incompressible flow, Hashiguchi and Kuwahara[7] proposed a new multi-directional third-order upwind finite-difference scheme. This scheme had already been applied by Suito et al.[8] to the study of the dynamic stall phenomena on the NACA0012 airfoil, and it had successfully predicted the hysteresis of the lift force against the angle of attack of the above mentioned airfoil.

In this paper, the flow field around a circular cylinder is numerically investigated by using the multi-directional third-order upwind finite-difference scheme for a wide range of Reynolds number,Re = 0.1 −

10^6. The flow is assumed to be: 1) two-dimensional, which remove the vortex stretching effect from the real fluid motion. It also reduces the real flow situation, which is essentially three-dimensional, to very limited situation. 2) described by the Navier-Stokes equations, which allows its numerical investigation. 3) generated by an impulsive start of the circular cylinder. According to the Kelvin's theorem, the vortex is shed into the main stream only from the viscous boundary layer developed on the cylinder surface. This fact will enable us to discuss the flow characteristics from a quite simplified point of view.

This paper is organized as follows: In section 2, mathematical formulation carried out, the governing equations and the discretization method are explained. In section 3, the computational results are compared with the data available in the literature. It will throughly validated the present numerical method. Lastly, conclusion is followed in section 4.

2. Numerical method

In this section, the methodology employed to obtain the numerical solutions for the flow field past a circular cylinder is presented.

2.1 Governing equations

Newtonian fluids governed by the incompressible Navier-Stokes equations of motion are considered. Under these conditions, the resulting dimensionless equations are:

$$\partial u^i/\partial t + u^j \partial u^i/\partial x^j = -\partial p/\partial x^i + Re^{-1}\partial^2 u^i/\partial x^j \partial x^j, \tag{1}$$

$$D = \partial u^i/\partial x^i = 0, \tag{2}$$

$u^i (i = 1, 2)$ being the velocity vector components in the Cartesian coordinate system x^i, p the pressure and t the time. $Re = u_\infty d/\nu$ is the Reynolds number where u_∞ is the free stream velocity, d is the cylinder diameter and ν is the kinematic viscosity, respectively. The variables are nondimensionalized with respect to d, u_∞, d/u_∞ and $Q = \rho u_\infty^2$ as the scales for length, velocity, time and pressure, respectively. Because it is difficult to solve the continuity equation (2) directly, a Poisson equation for the pressure is derived. The Poisson equation is described by

$$\partial^2 p/\partial x^i \partial x^i = -(\partial u^i/\partial x^j)(\partial u^j/\partial x^i) + D^n/\triangle t, \tag{3}$$

where the index n stands for the previous time step and D is the divergence of the velocity field(See Eq.(2)). The time derivative term, which appears in the right hand side of Eq.(3) , is maintained as a numerical correction term in accordance with the MAC mtehod. The solution of this equation satisfies the continuity equation at time step $n+1$ ($D^{n+1} = 0$).

The velocity field is initially set to the free-stream velocity over the entire domain. The associated boundary condition for the velocity field is the no-slip conditin on the cylinder surface. The value of pressure on the surface is imposed by setting the normal derivative of the pressure to zero.

2.2 Finite-difference method

Equations (1),(2) and (3) are transformed into a generalized coordinate system and then discretized based on the finite-difference method. The multi-directional finite-difference method proposed by Hashi guchi and Kuwahara[7] is used for the spatial discretization. This method was developed in order to remove numerical inaccuracy due to velocity component skewness against the grid arrangement. We explain the method briefly. Consider a grid system in physical domain as shown in Fig.1. We can define two observer systems A and B on the grid system. Each system is mapped onto a different computational domain, and its equations are discretized independently. The velocity and pressure are defined on the same grid point. Second-order central finite-difference approximations are used for the spatial derivatives excluding the nonlinear convection term in the Navier-Stokes equations. For the convection term, the third-order upwind scheme is used.

$$\begin{aligned} f\partial u^i/\partial \xi &= f_{ij}\{-(u_{i+2j} - u_{i-2j}) + 8(u_{i+1j} - u_{i-1j})\}/(12\triangle\xi) \\ &+ \alpha|f_{ij}|\{(u_{i+2j} + u_{i-2j}) - 4(u_{i+1j} + u_{i-1j}) + 6u_{ij}\}/(12\triangle\xi) \end{aligned} \tag{4}$$

The weight α of the numerical dissipation part in Eq.(4) is set to 3 according to Kawamura and Kuwahara[4]. The finite-difference approximation obtained in system A and system B are combined with the weight ratio of 2:1. This ratio was determined by requiring that the leading error term of the resultant

finite-difference approximation of Eq.(2) has the Laplacian form. This requirement ensures the rotational invariance of the mass conservation in the coordinate transformation. It is also easy to prove that the resultant finite-difference approximation of the Laplacian in Eqs.(1) and (3) has the leading error term of the double Laplacian form which is indeed rotational invariant. The second-order Crank-Nicolson scheme is used for the discretization of the time derivative. A O-type grid is used with the grid points concentrated near the cylinder surface.

2.3 Flow visualization system

For an unsteady flow computaton, the output data is so huge that it is hard to extract meaningful information related to the time evolution of the flow structures without the help of an efficient visualization system. For the present computations, the animated graphics system Globe2D(developed by Kuzuu et al. [9]) was utilized. Globe2D uses Open GL as a graphics language and can run under Windows NT. Globe2D allows for a real-time visualization of the essentially unsteady flow field around a circular cylinder that enables us a better understanding of the different flow patterns. Flow computation and real-time visualization are performed on a high-performance PC (600 MFLOPS) running on a Windows NT environment.

3. Results and discussion

First, the aerodynamic coefficient of drag C_D, which is defined as $C_D = Drag/(0.5Qd)$, is predicted and compared with experimental results. The number of grid points used are 32×16 , 64×32 and 128×64. The O-type grid arrangement is shown in Fig.2. The radius of outer boundary is set to more than $30d$. A wide range of Reynolds number, $0.1 \leq Re \leq 10^6$, was studied. The dependence of C_D is predicted as shown in Fig.3. If the Reynolds number is in the range of 0.1 to 1, the present computation agrees with the analytic solution obtained by Tomotika and Aoi[10]. They used the Oseen approximation while the present scheme integrated the full Navier-Stokes equations. For $1 \leq Re \leq 100$, all the computations and experiments[11][12] agree very well. At high Reynolds numbers, even 64×32 computation can reproduce the drag crisis qualitatively. The 128×64 computations agrees much better with the experiments [12] as expected. The drag sharply decreases at about Reynolds number $400,000$, which is called drag crisis, is well captured even using this coarse grid, while Tamura and Kuwahara[5] used the large number of grid points 400×100. Although the predicted C_D has still higher value than that of the experiment for $10^3 \leq Re \leq 10^4$, the validity of the present method will become more clear after the examination of computed time-averaged streamlines as shown later in Fig.5. The instantaneous streamlines at different Reynolds number are shown in Fig.4. For very small Reynolds number (Re = 0.1 and 7), as shown in Fig.4a-b, the streamlines are steady and present a very good agreement with Taneda's experimental observation[13]. On the other hand, for higher Reynolds number (Re = 100, 10^4, and 10^5), as shown in Fig.4c-e, the streamlines vary due to the flow unsteadiness. When the Reynolds number is further increased, the unsteady vortex shedding becomes more visible. Time-averaged streamlines are shown in Fig.5 to clarify the effect of the Reynolds number on: (i) the position of the separation points, and (ii) the size of the wake region. Figure 5a-b($Re = 10^4$ and 10^5, respectively) shows the upstream location of the time-averaged separation points before the drag crisis occurs. After the Reynolds number is increased(leading to the occurence of the drag crisis), the location of the separation point is shifted downstream and the wake size contracts as shown in Fig.5d($Re = 10^6$). This result coinsides with the qualitative explanation for the drag crisis. Furthermore, the present computation is the first to capture the stationary deflected flow pattern and asymmetry location of the separation points as shown in Fig.5c($Re = 5\times10^5$). This interesting phenomenon has been reported experimentally by Kamiya et al.[14]. The corresponding time-averaged surface pressure distributions were also examined, and the results are presented in Fig.6. The pressure distribution for the potential flow is included for comparison. It clearly shows that a very high Reynolds number flow can be modeled as a potential flow. As for the case of stationary deflected flow pattern, Fig.6.c($Re = 5\times10^5$), the asymmetric pressure distributions results in a stationary lift force for this case.

Moreover, the Strouhal number St was estimated from the time history of the lift coefficient C_L for four different Reynolds number ($Re = 10^4, 10^5, 5 \times 10^5$ and 10^6), taking on the values 0.19, 0.24, 0.28 and 0.3, respectively. These values agree well with the experimental results cited by Ikui et al.[15].

Therefore, it can be concluded that the present computations systematically predict C_D and the related flow characteristics for a wide range of Reynolds number($Re = 0.1 - 10^6$) without any turbulence model. Based on the observation of the time-averaged stream lines and surface pressure distribution for $Re = 10^6$, it can be stated that the most simple explanation for the change of C_D and the flow pattern

at the drag crisis, is merely the approach to the potential flow rather than the effect of turbulence.

Here, a question can be raised: How do the flow approach the potential flow characteristics ? Such an answer is not straightforward. A step in the right direction is to examine how the vortices are being shed from the boundary layer on the cylinder surface. Fig.7, 8 and 9 ($Re = 100$, 1200 and 10^5, respectively) show the time evolution of the separated shear layer and the unsteady vortex shedding just after the impulsive start. The 256×128 computations were executed. Because of the impulsive start, the initial flow field is potential flow for all these cases and is eating up by the vortices shed from the cylinder surface. In Fig.9, time evolution of the separated shear layer or vortex shedding at $Re = 10^5$ is quite different when compared to the others. Fig.9 also shows that the vortices being shed from the cylinder surface are swept out downstream and the remaining flow structure resembles that of a potential flow. This fact suggests that the penetration of the vorticity shed from the cylinder surface into the main potential flow field will characterize the flow patterns.

4. Concluding remarks

The flow field around a circular cylinder was numerically investigated based on the multi-directional third-order upwind finite-difference method. The Navier-Stokes equations were solved directly without any explicit turbulence model. As a result, it was found that the present method can reproduce the essential features of the flow past a circular cylinder for a wide range of $Re = 0.1 - 10^6$, including the drag crisis. From the examination of the vortex shedding just after the impulsive start, it is suggested that the depenence of the vortex shedding pattern on the Reynolds number shall be investigated in detail in order to clarify the mechanism of the change of the flow pattern at the critical flow regime.

Acknowledgement

The authos would like to thank Dr.Angel M. Bethancourt of the Institute of Computational Fluid Dynamics for his helpful discussion on this paper.

References

(1) Thom,A., Proc.Roy.Soc.London, A141(1933), 651.
(2) Kawaguti,M., J.Phys.Soc.Japan, Vol.8, No.6(1953), 9.
(3) Payne,R.B., J.F.M. 4(1958),81.
(4) Kawamura,T. and Kuwahara,K.,AIAA paper No.840340(1984) .
(5) Tamura,T. and Kuwahara,K., Int. Sympo. on Compu. Fluid Dynamics Nagoya-1989(1989).
(6) Ishii,K.et al., AIAA paper No.851660(1985).
(7) Hashiguchi,M.and Kuwahara,K.,6th CFD symposium(1993),567.
(8) Suito,H. et al., AIAA paper No.952264(1995).
(9) Kuzuu,K. et al.,AIAA paper No.970235(1997), to be appeared.
(10) Tomotika,S.and Aoi,T.,Quart.J.Mech. 4 (1951),401.
(11) Tritton,D.J.,J.F.M. Vol.6,part.4(1959),547.
(12) Wieselsberger,C.,Phys.Z. Vol.22 (1921),321.
(13) Taneda,S., Fluid Dynamics, Asakura-shoten(1988),31.
(14) Kamiya,S. et al.,AIAA paper No.791475(1979).
(15) Ikui,T.and Inoue,M.,Dynamics of Viscous Fluid, Rikogakusha(1994),227.

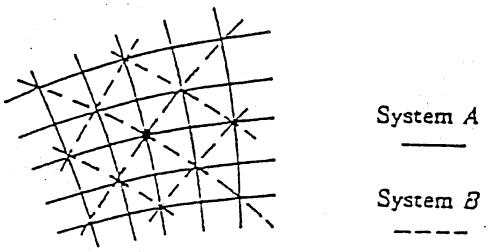

Fig.1 Grid system and observers A and B.

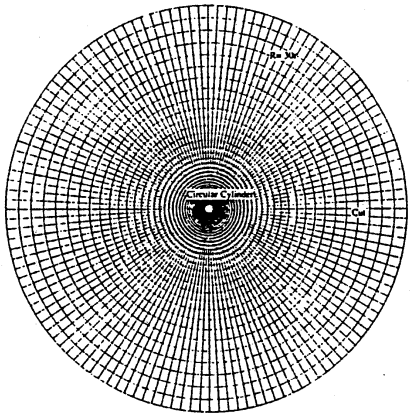

Fig.2 O-type grid system.

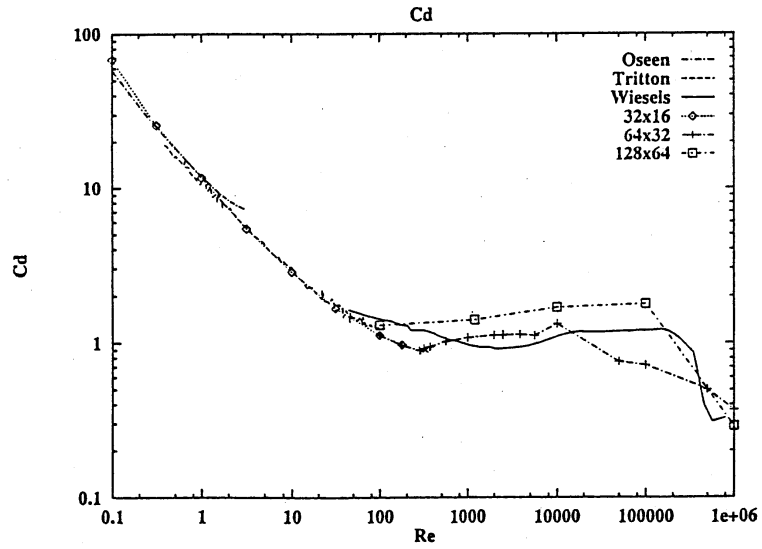

Fig.3 Dependence of C_D on Reynolds number.

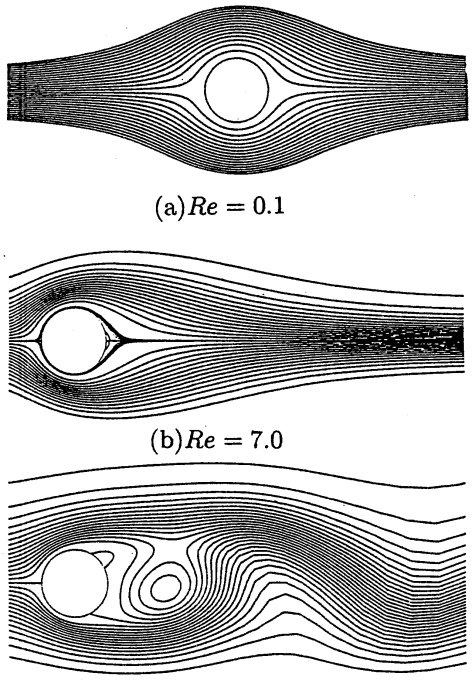

(a)$Re = 0.1$

(b)$Re = 7.0$

(c)$Re = 10^2$

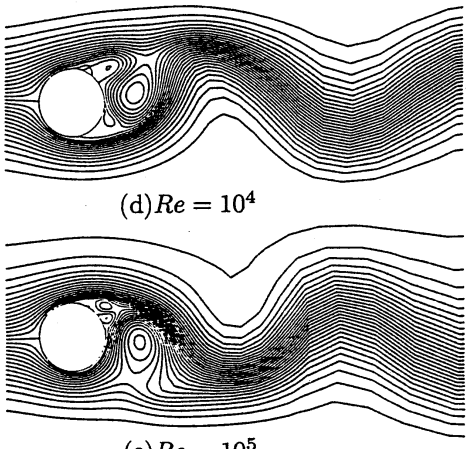

(d)$Re = 10^4$

(e)$Re = 10^5$

Fig.4 Instantaneous streamlines.

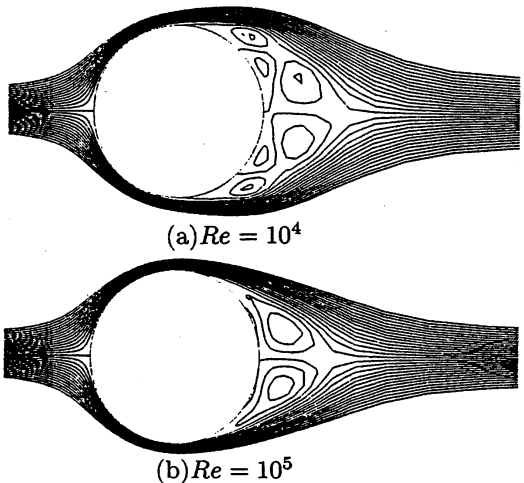

(a)$Re = 10^4$

(b)$Re = 10^5$

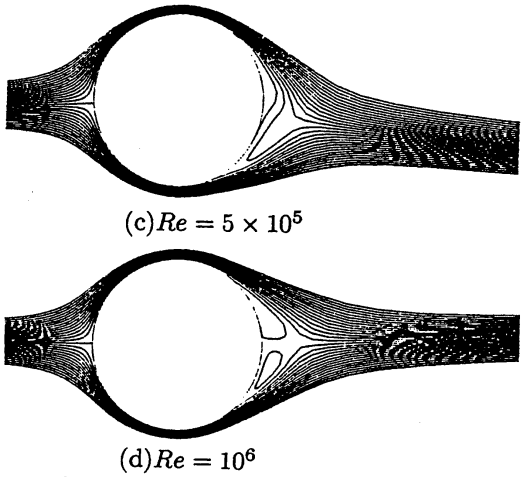

(c)$Re = 5 \times 10^5$

(d)$Re = 10^6$

Fig.5 Time-averaged streamlines.

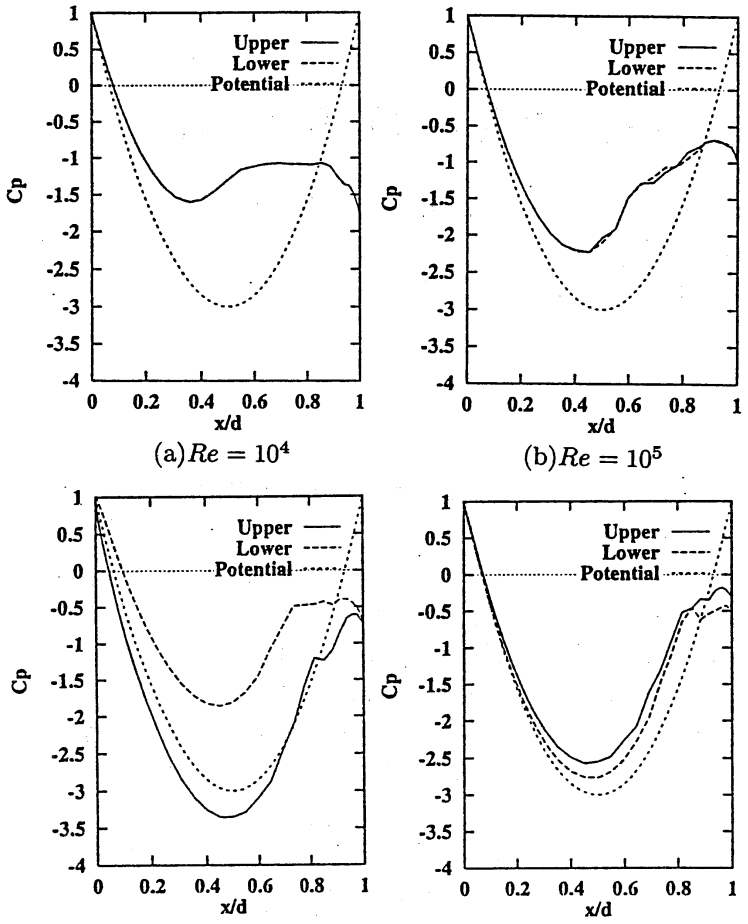

(a)$Re = 10^4$ (b)$Re = 10^5$

(c)$Re = 5 \times 10^5$ (d)$Re = 10^6$

Fig.6 Time-averaged pressure distributions; $C_p vs. x^1/d$.

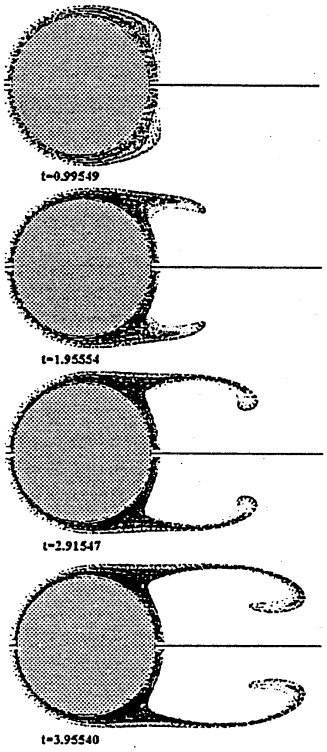

Fig.7 Particle path; $Re = 100$.

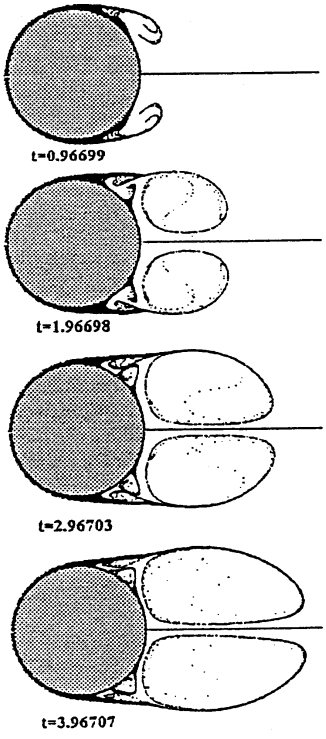

Fig.8 Particle path; $Re = 1200$.

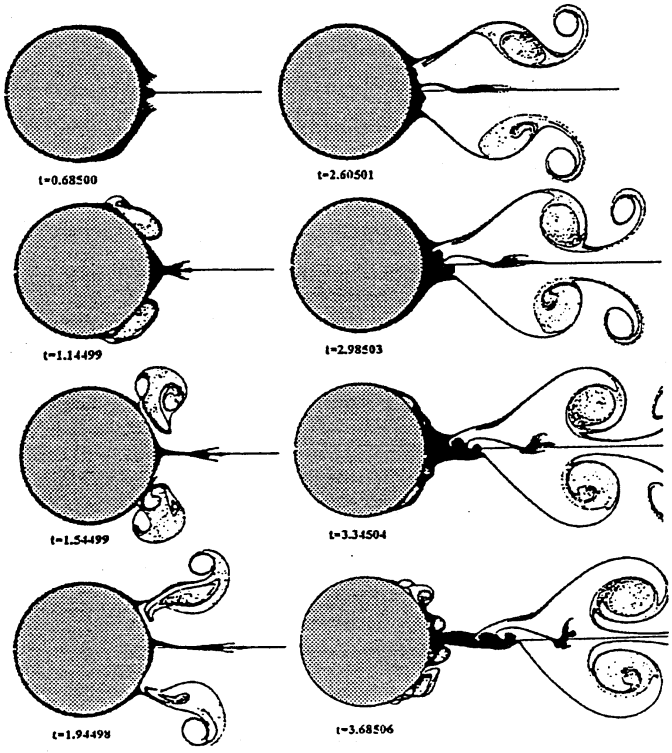

Fig.9 Particle path; $Re = 10^5$.